RSC Advances

PAPER

View Article Online
View Journal | View Issue

Cite this: *RSC Adv.*, 2022, **12**, 33099

Improvement and regeneration of Co–B amorphous alloy nanowires for the selective hydrogenation of cinnamaldehyde

Min Mo, * Jiansheng Tang, Lijun Zou, Youyi Xun and Hongru Guan

One-dimensional Co–B amorphous alloy nanowires (NWs) were prepared using surfactant as a template and were treated with plasma to study the effect of different treatment times on the essential physical and chemical properties of the catalyst. The study showed that plasma with a certain amount of strength will not change the morphology and amorphous structure of the NWs within the chosen treatment time. It could, however, modify the electronic structure and active sites of the catalyst surface, increase its specific surface area and H_2 adsorption capacity, and also improve the selective hydrogenation performance of cinnamaldehyde. Most of all, plasma treatment could also play an important role in the reuse of catalysts. After several recycling reactions, plasma treatment on Co–B amorphous alloy NWs could regenerate their high catalytic activity. This work provides a novel method for preserving the high catalytic activity and stability of amorphous alloy nanomaterials, as well as for increasing their reusability.

Received 5th September 2022
Accepted 4th November 2022

DOI: 10.1039/d2ra05595c

rsc.li/rsc-advances

1. Introduction

The selective catalytic hydrogenation of cinnamaldehyde (CMA) that is representative of the bond coupling in C=C and C=O bonds of α,β-unsaturated aldehydes is appealing to both academic and industrial fields.[1–4] In CMA, hydrogenation that occurs at C=O could produce unsaturated cinnamyl alcohols (CMO), while at C=C it could yield saturated dihydrocinnamaldehydes (HCMA). These products are followed by total hydrogenation to 3-phenylpropanol (HCMO) (Fig. 1).[5,6] CMO could be an important hydrogenation product owing to its important applications in flavors, pharmaceutical intermediates, and fragrances. However, the reduction of the C=C group is thermodynamically more favorable than that of the C=O group, and thus, it has attracted considerable attention that has led to the designing of catalysts with an ideal selectivity for CMO.[7,8] To obtain CMO, various catalysts have been developed. Catalysts based on noble metals (Ru, Pt, Rh, and Pd) or a combination of noble and transition metals (Pt–Co, Pt–Fe, *etc.*) are highly reactive; however, they have poor selectivity for CMO.[2,9] To improve their selectivity, the physicochemical properties of these catalysts (such as the metal atoms, the electronic effect of the second metal, surface ligands, local structure, as well as texture of the support) have been addressed.[10–15]

The cost of a catalyst is a core concern in industrial catalysis; thus, it is necessary to develop low-cost and highly active hydrogenation catalysts to alleviate the demand for noble metals.[16–20] Nonprecious metal catalysts, such as Co–B amorphous alloys, are excellent hydrogenation catalysts for CMA owing to their low cost, easy access, and excellent selectivity for CMO.[21,22] Although there are also some disadvantages to them, such as the reduction of catalytic activity due to agglomeration, oxidation by oxygen in the air, *etc.* Nanoscale granular Co–B amorphous alloy catalysts can be easily obtained by wet chemical methods without using a surfactant as a template as the reaction between Co^{2+} and reducing agents (such as BH_4^-) is violent and can cause particle agglomeration. In addition, granular amorphous alloys easily agglomerate during the catalytic hydrogenation reaction, thereby reducing their catalytic activity.[23,24] Moreover, Co–B amorphous alloy catalysts are easily oxidized by oxygen in the air, leading to deactivation in their

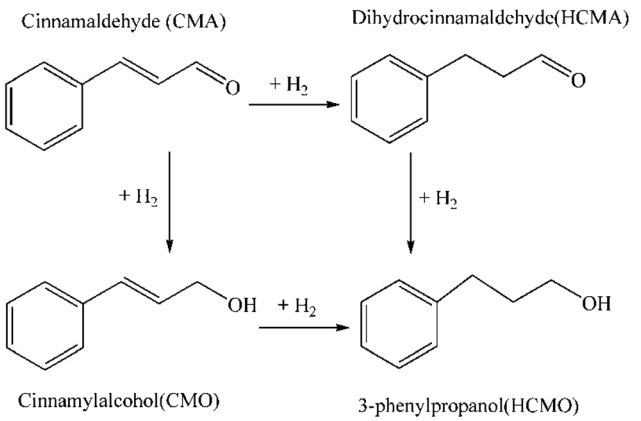

Fig. 1 Possible reaction pathways for hydrogenation of CMA.

School of Physics and Chemistry, Hunan First Normal University, Changsha 410205, China. E-mail: momin320@126.com; Fax: +86 731 82841070; Tel: +86 731 82841012

CMA hydrogenation performance. Determining a method to overcome this degradation of catalytic performance due to agglomeration and oxidation, and improve the reusability is a challenge. Preference has been given to research geared toward the synthesis of amorphous alloy catalysts with nanotube,[25–27] nanosphere,[28–30] and nanochain[22] morphologies, which can effectively prevent agglomeration and enhance the structural stability of nanocatalysts. We previously reported a series of one-dimensional (1D) amorphous alloy nanotubes with high catalytic hydrogenation activity and selectivity by using the layered liquid crystal template method. However, there was no significant progress in the oxidation resistance of the amorphous alloy catalysts.

As an effective molecular activation technology, low-temperature plasma is increasingly used in catalyst preparation and reaction.[31,32] Plasma technology is a low-energy process, which is regarded as an efficient tool for preparing or modifying materials. It is environmentally friendly as it does not produce solvent and chemical waste. Plasma surface treatment can change the valence state of metal active components to achieve catalyst reduction, and greatly optimize the physicochemical properties of catalysts. Plasma technology is widely used to treat electrocatalysts at room temperature.[33–35] However, only a few studies have reported the effect of plasma treatment on amorphous alloy catalysts for the enhancement of catalytic hydrogenation performance. In this study, we synthesized a 1D Co–B amorphous alloy catalyst with nanowire morphology which has higher structural stability and longer catalytic lifetime compared to granular and tubular counterparts. The effect of plasma treatment on the morphology, physicochemical properties of amorphous alloy catalysts, and the improvement of the selective hydrogenation performance of CMA were studied. Moreover, in the recycling catalytic process of the Co–B amorphous alloy catalyst, the degradation of catalytic hydrogenation performance caused by the oxidation of the catalyst surface due to unavoidable contact with air could also be regenerated by plasma treatment after a certain number of cycles, which provides convenience for the application of amorphous alloy catalysts for catalytic hydrogenation.

2. Experimental

2.1 Sample preparation

The Co–B amorphous nanowires (NWs) were prepared as follows: Tween 80 (0.005 mol), camphor sulfonic acid (CSA, 0.0025 mol) was dissolved in 12 mL of deionized water in a water bath at 343 K while stirring evenly. 0.005 mol of $CoCl_2 \cdot 6H_2O$ was then added to the above solution and constantly stirred until a transparent and homogeneous solution was formed. The resultant solution was placed in a water bath and slowly cooled from 343 to 298 K, after which a mixture of $NaBH_4$ (4 mol L^{-1}) and NaOH (0.1 mol L^{-1}) was pumped into the system while stirring in a nitrogen atmosphere. After completion of the reaction, the resultant solution was aged for 36 h. A black precipitate was obtained, which was cleaned thrice with deionized water and anhydrous alcohol. It was then dried in an N_2 atmosphere. This sample of amorphous alloy NWs was labeled Co–B-0 NWs.

Low-temperature plasma treatment was performed on amorphous alloy catalysts as follows: Co–B NWs prepared were placed on a quartz boat in a plasma reactor after which they were treated using argon plasma of 200 W power for 100, 200, and 300 seconds. The samples obtained were labeled Co–B-100 NWs, Co–B-200 NWs, and Co–B-300 NWs, respectively.

2.2 Characterization

The morphology of the Co–B NWs was inspected using transmission electron microscopy (TEM; JEM-1011) with an accelerating voltage of 120 kV. Their crystal structure was measured using powder X-ray diffraction (XRD; Philips). Their chemical compositions and electronic states were studied using X-ray photoelectron spectroscopy (XPS; Thermo ESCALAB 250). The nitrogen-sorption isotherms of the Co–B NWs were characterized using the ASAP 2020 apparatus. H_2 temperature programmed desorption was tested by using an apparatus (H_2-TPD; AutoChem TP-5080) with a thermal conductivity detector.

2.3 Catalytic test

The catalytic performance of the Co–B amorphous alloy NWs was evaluated as follows: 0.3 g of catalyst, 2 mL of CMA, and 170 mL of absolute ethanol were added into a 200 mL reactor. After purging thrice with N_2 and H_2 while stirring, hydrogen at a predetermined pressure of 1.0 MPa was introduced into the system. These conditions were maintained throughout the reaction process. The reactor was heated to 373 K, which marked the beginning of the reaction time. As the reaction proceeded, samples were removed from the reactor regularly and analyzed using gas chromatography (GC-2014 Shimadzu). The conversion of CMA and selectivity of the products were calculated using the following formula:

$$\text{Conversion}\ (\%) = \left(1 - \frac{\text{moles of residual CMA}}{\text{moles of initial CMA}}\right) \times 100\%$$

$$\text{Selectivity}\ (\%) = \frac{\text{moles of product}}{\text{moles of reacted CMA compound}} \times 100\%$$

3. Results and discussion

3.1 Characteristics of nanowires

As shown in Fig. 2(a) and (b), the Co–B-0 NWs were uniform in morphology, approximately 2–5 μm in length and 35–45 nm in diameter. Fig. 2(c) and (d) shows TEM images of the Co–B-200 NWs. Their morphology was maintained after plasma treatment. The Co–B-200 NWs were 1–4 μm in length and 30–40 nm in diameter. This indicated that plasma treatment had little effect on the morphology of NWs. The selected area electron diffraction (SAED) inserted in Fig. 2(b) and (d) implied that the structure of Co–B-0 and Co–B-200 NWs was amorphous.

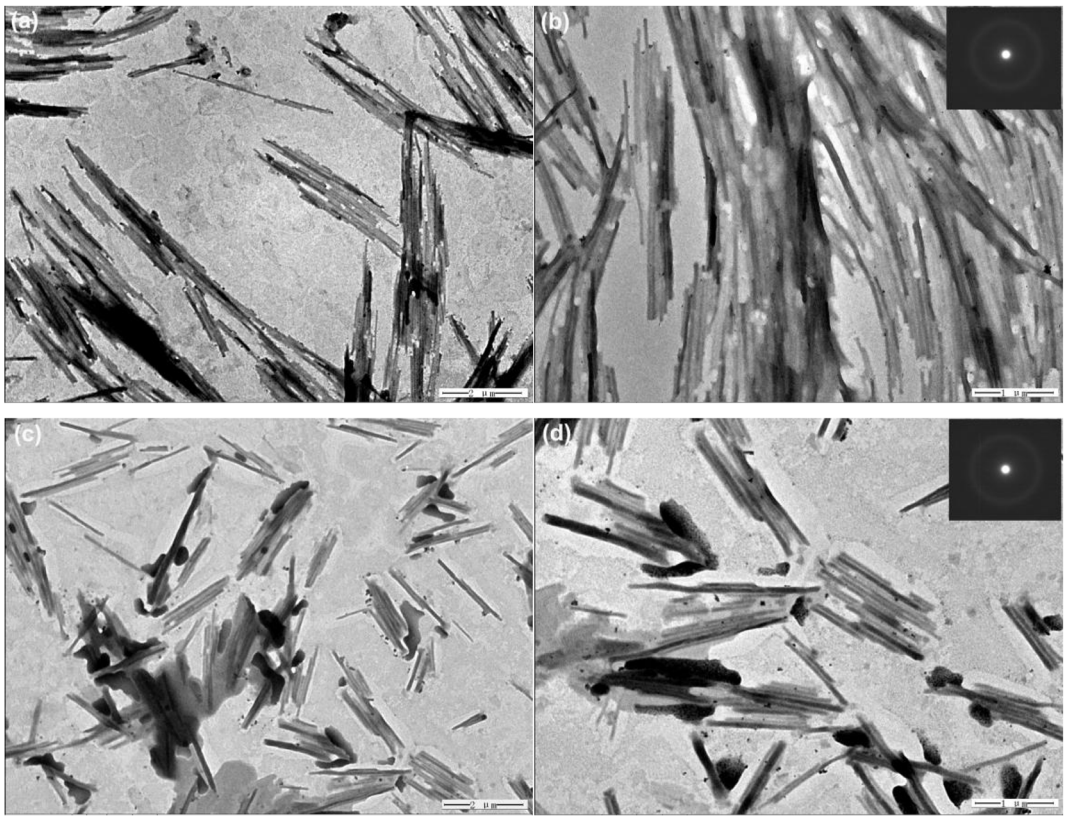

Fig. 2 TEM images of (a and b) Co–B-0 NWs at different magnifications and (c and d) Co–B-200 NWs.

Co–B-0 NWs were prepared by reducing Co^{2+} in the water layer of layered liquid crystal with sodium borohydride. The lamellar liquid crystal was formed of Tween 80, camphor sulfonic acid (CSA), and cobalt salt dissolved in water after cooling from 348 to 298 K. Fig. 3(a) shows the small-angle XRD pattern of the layered liquid crystal. The layer spacing is 9.85 nm. When the layer spacing was relatively smaller, such as d = 7.37 nm as previously reported,[25] the amorphous alloy nanotubes were easily formed through the curling mechanism.[25–27] However, in this work, it was easy to form NWs because the layer spacing was large (d = 9.85 nm), and the lamellar liquid crystal could not be curled. The Co–B amorphous alloy NWs were confined to formation in the water layer of the liquid crystal. The wide-angle XRD spectra of Co–B-

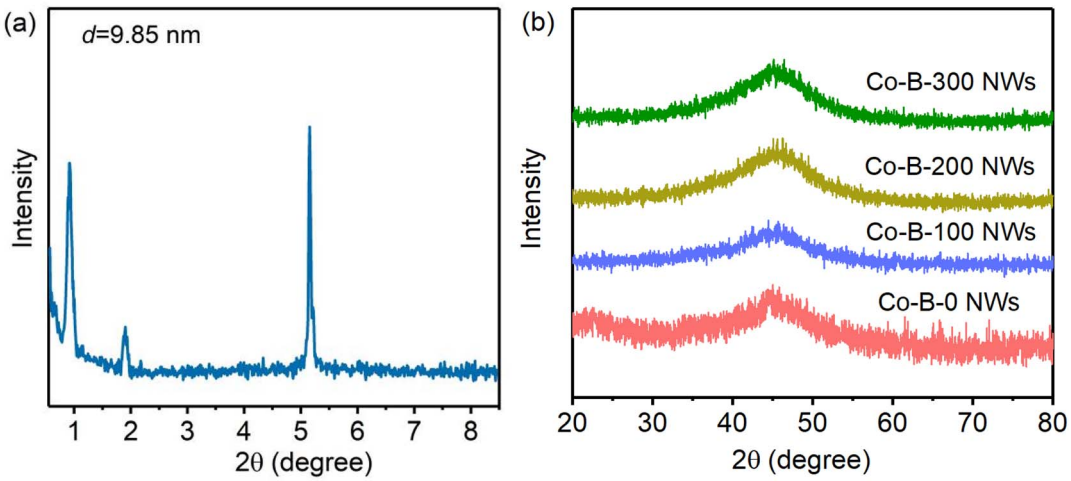

Fig. 3 (a) Small-angle XRD patterns of the liquid crystals with Tween 80/CSA/Co^{2+}(H_2O), and (b) XRD of Co–B NWs treated with plasma at different times.

0 NWs, Co–B-100 NWs, Co–B-200 NWs, and Co–B-300 NWs in Fig. 3(b) show amorphous structure, indicating that plasma treatment on Co–B NWs did not change the crystal structure of the amorphous alloy NWs.

Fig. 4 shows the XPS spectra of Co–B-0 NWs and Co–B-200 NWs. The Co $2p_{3/2}$ deconvolution for Co–B-0 NWs is demonstrated in Fig. 4(a). The elemental state was at 777.5 eV, while that of CoO and $Co(OH)_2$ was at 779.6 and 781.1 eV, respectively. The peak at 782.9 eV was attributed to the electron shakeup peak for $Co(OH)_2$ multiple splitting.[36,37] The deconvolution of the B_{1s} spectrum for Co–B-0 NWs is shown in Fig. 4(b). The peaks for B_{1s} at 187.9 and 192.1 eV corresponded to elemental and oxidized B, respectively.[38–40] Notably, the binding energy of elemental B in Co–B-0 NWs shifted positively by approximately 0.8 eV compared to the binding energy of pure B at 187.1 eV, which indicated that B partially donated electrons to the alloyed Co. The electron transfer between Co and B in Co–B NWs made Co electron-rich and B electron-deficient.[22,36] The electron-rich Co in Co–B was then able to facilitate the catalytic reaction of CMA to CMO.[22] The composition of Co–B-0 NWs from XPS data was $Co_{72.1}B_{27.9}$. The deconvolution of Co $2p_{3/2}$ and B_{1s} spectra of Co–B-200 NWs was similar to that of the Co–B-0 NWs except that the binding energy of Co had a small negative shift of approximately 0.1 eV, whereas the binding energy of B had a positive shift of approximately 0.6 eV. The relative peak areas for the elemental and the oxidation states in the XPS spectra changed. The relative proportions of each species of all samples are listed in Table 1. As the electron shakeup peak of $Co(OH)_2$ at 782.9 eV was not incorporated in calculations, the sum of the peak areas of Co^0 and Co^{2+} was not 100%.[36] When the plasma treatment time was 100 and 200 seconds, the relative content of Co^0 and B^0 increased significantly; however, the increase in the zero-valence species content of Co–B-300 NWs was not obvious as compared with that of Co–B-200 NWs. Research has shown that the higher the content of elemental Co and B, the greater the electron transfer and the faster the reaction.[36–38] In summary, the result indicated that the synergistic effect between Co and B was enhanced after plasma treatment.

Fig. 5(a) shows the nitrogen adsorption isotherm and pore size distribution curves for Co–B-200 NWs, while the specific surface and pore volume data for all samples are listed in Table 1. The results show that the Co–B-200 NWs maintained their mesoporous structure after plasma treatment.[27] However, the treatment increased the specific surface and pore volume of the Co–B NWs. The H_2-TPD curves for Co–B-0 and Co–B-200 NWs are shown in Fig. 5(b), and the H_2 uptake for all the samples are listed in Table 1. The TPD peak for Co–B-200 NWs moved toward a higher temperature as compared with that for Co–B-0 NWs, indicating that plasma treatment on Co–B NWs was conducive to the stronger adsorption of H_2 on the catalyst. Notably, the surface active site of Co–B-200 NWs was more uniform, which may promote the selectivity of catalytic hydrogenation reaction.[23] Moreover, the samples with plasma treatment had a higher H_2 uptake than the Co–B-0 NWs.

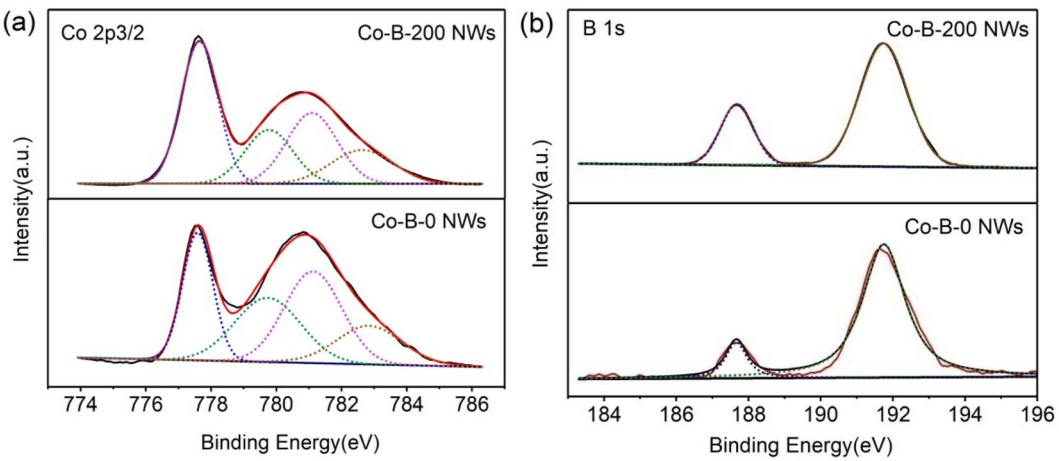

Fig. 4 Peak deconvolution of (a) Co $2p_{3/2}$, (b) B_{1s} level for amorphous Co–B-0 and Co–B-200 NW powders.

Table 1 The relative peak areas in the XPS spectra with a summary of essential chemical and physical properties

	Co $2p_{3/2}$		B_{1s}				
Catalyst	Co^0	Co^{2+}	B^0	B^{3+}	S_{BET} ($m^2\ g^{-1}$)	Pore volume ($cm^3\ g^{-1}$)	H_2 uptake ($\mu mol\ g^{-1}$)
Co–B-0	24.4%	56.3%	11.9%	88.1%	82.9	0.51	56.1
Co–B-100	30.1%	52.1%	20.7%	79.3%	88.7	0.60	60.8
Co–B-200	38.9%	53.0%	25.8%	74.2%	92.4	0.61	74.0
Co–B-300	39.1%	53.1%	26.2%	73.8%	89.5	0.60	73.8

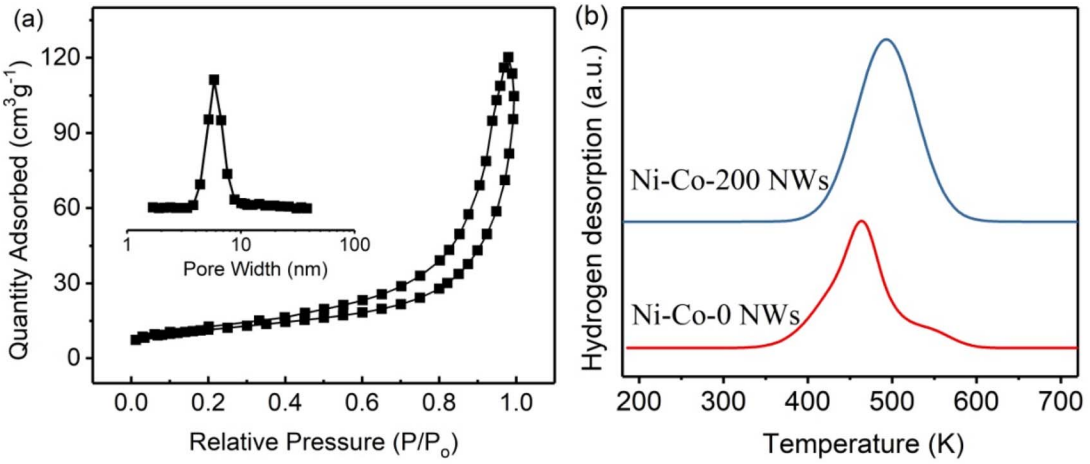

Fig. 5 (a) N_2 adsorption isotherms and pore size distribution curves for Co–B-200 NWs, and (b) H_2-TPD curves for Co–B-0 NWs and Co–B-200 NWs.

3.2 Catalytic property for hydrogenation of CMA

Fig. 6 demonstrates the time-dependent curves for the conversion of CMA and product selectivity for CMO, HCMA, and HCMO for all samples. It can be observed from Fig. 6 that the target product (CMO) was the main product of the CMA hydrogenation reaction, although it was accompanied by the formation of by-products. For the Co–B-0 NWs catalyst (no plasma treatment), the complete conversion of CMA took 6

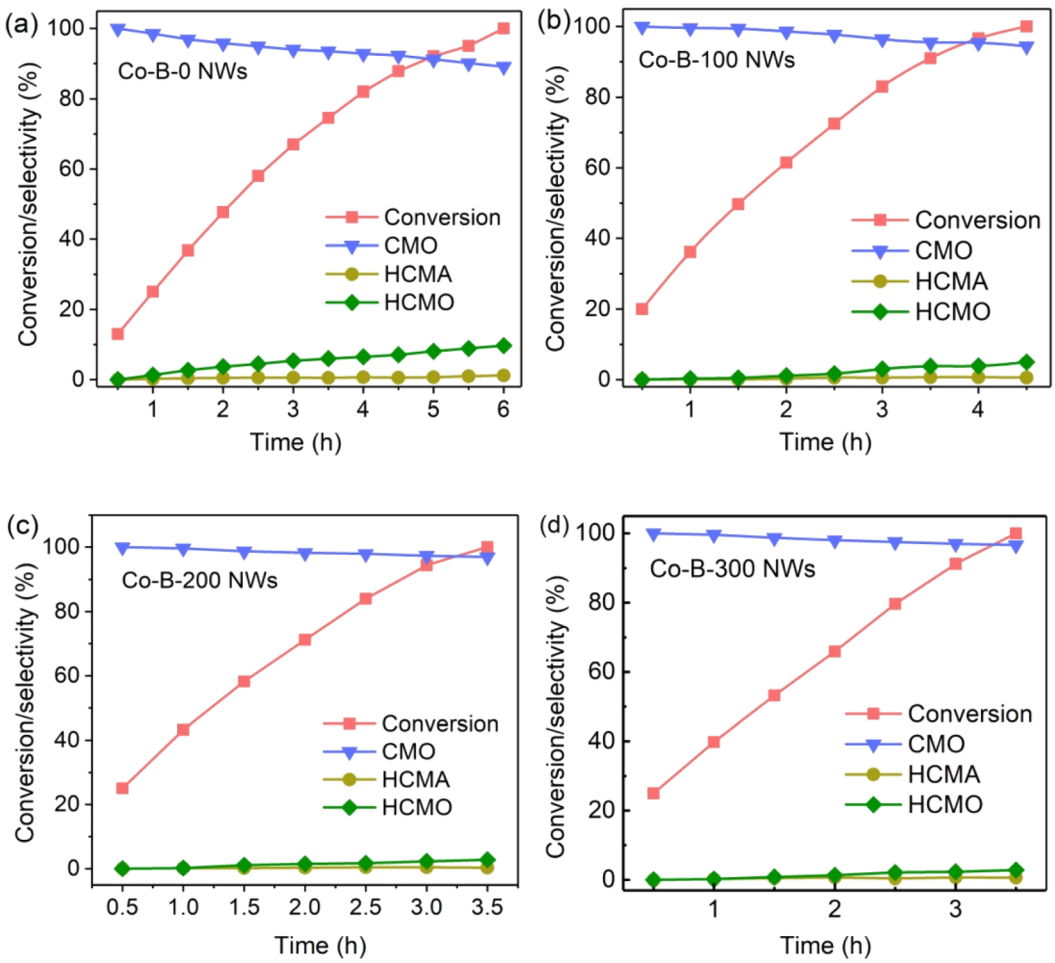

Fig. 6 Reaction profiles of CMA hydrogenation on (a) Co–B-0 NWs, (b) Co–B-100 NWs, (c) Co–B-200 NWs, and (d) Co–B-300 NWs.

hours, and the final selectivity for CMO was only 89.1%. We also studied the impact of plasma treatment time on the catalytic reaction. It was found that the catalytic performance of Co–B NWs improved greatly after plasma treatment. For Co–B-100, Co–B-200, and Co–B-300 NWs, the time for the complete conversion of CMA reached 4.5, 3.5, and 3.5 h, respectively, and the selectivity for the main product (CMO) was 94.4, 96.9, and 96.6%, respectively. As compared with Co–B-200 NWs, the catalytic performance of Co–B-300 NWs did not improve significantly, indicating that after a certain time (200 s in this case), the effect of plasma treatment on Co–B NWs could not be improved by simply prolonging the plasma treatment time.

The selective hydrogenation mechanism of cinnamaldehyde under Co–B NWs could be depicted as follows. The high CMA catalytic activity of Co–B NWs was due to the structural and electronic effect.[9–11] Structurally, Co–B amorphous alloy NWs that were long-range ordered and short-range disordered were very beneficial to the hydrogenation reaction. The highly unsaturated and dispersed Co active sites that were fully exposed and the strong interaction between different Co active sites could improve the hydrogenation activity. From the perspective of electronic effect, the alloyed B in the Co–B NWs transferred some electrons to Co, making Co electron-rich, which was conducive to the hydrogenation reaction. The electron-deficient B was also instrumental in the adsorption of the C=O group on the catalyst.[41] The high CMO selectivity of the Co–B NWs catalyst may be due to the unwelcome contact and adsorption between the Co active site and the C=C group because the steric hindrance caused by the direct connection with benzene ring made the C=C group on CMA adsorb readily on the Co active site. At the same time, it promoted the adsorption of C=O on the catalyst surface, thus improving the hydrogenation selectivity of C=O.[21,22,25,41] The improvement in the catalytic performance of Co–B NWs with plasma treatment as compared with those of their untreated counterparts was achieved through the higher specific surface area and pore volume of the catalyst, homogeneous active sites, and higher hydrogen adsorption capacity, as well as the stronger synergistic effect of Co and B on the catalyst surface.

To study the sustainable utilization of catalysts, a recycling experiment was performed. The results are shown in Fig. 7. Fig. 7(a) shows the experimental results of six cycles on Co–B-200 NWs. Each catalytic reaction lasted for 3 h. After the reaction was completed, the conversion of CMA and the selectivity for CMO in the product were tested. During the first through to the fifth run of the recycling experiment, the catalyst

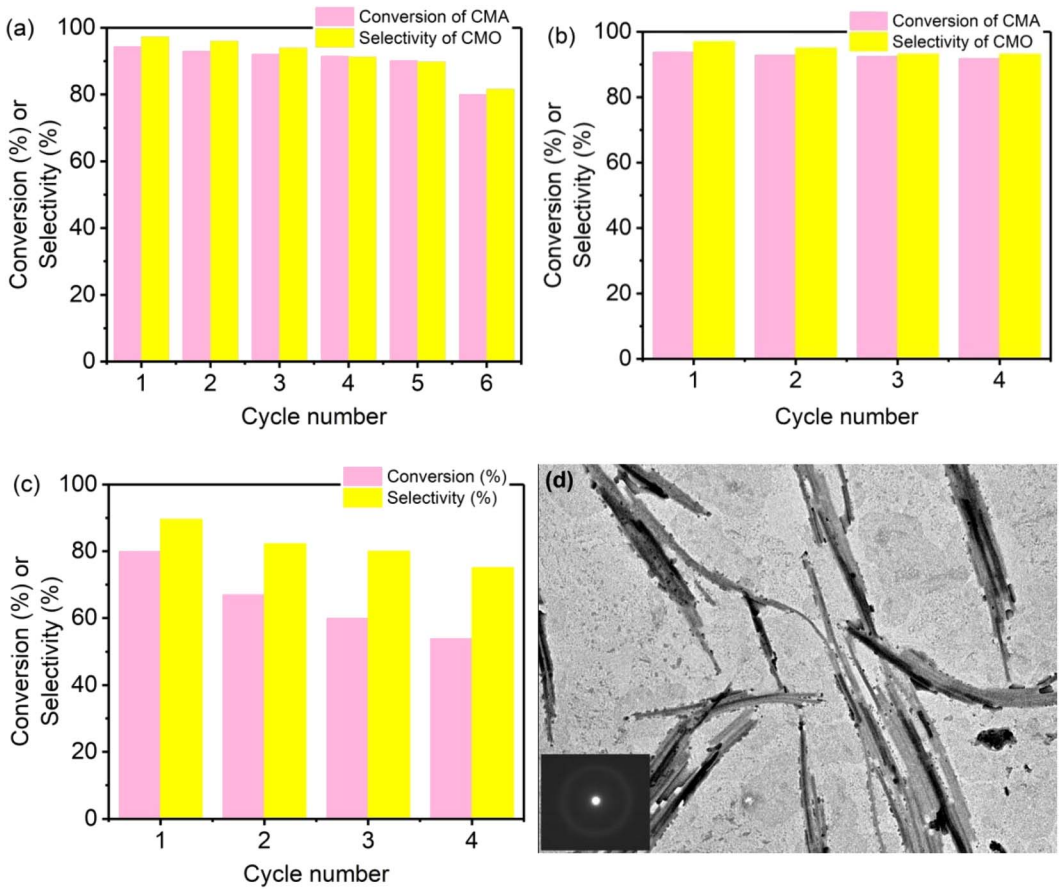

Fig. 7 (a) Conversion of CMA and selectivity of CMO on Co–B-200 NWs for 3 hours as a function of the number of times the catalyst was recycled, (b) catalytic performance of Co–B-200 NWs after the second plasma treatment, (c) catalytic performance on Co–B-200 NWs after the ninth plasma treatment, and (d) TEM image of Co–B-200 NWs after nine plasma treatments.

maintained high catalytic activity, but when it was recycled for the sixth time, its catalytic performance decreased significantly. The decline in catalytic performance may have resulted from the oxidation of the catalyst during experimental manipulation. To explore the effect of plasma treatment on the reusability of the catalysts, the Co–B-200 NWs were treated with plasma for 200 additional seconds after four cycles of catalytic reactions, where each lasted for 3 h. Fig. 7(b) shows the experimental results of four cycles of Co–B-200 NWs activity after the second plasma treatment. It can be observed that the catalyst retained high conversion and selectivity. However, after the ninth plasma treatment, the activity of the catalyst declined significantly as shown in Fig. 7(c). The TEM test results of the samples shown in Fig. 7(d) indicate that there were many nanoparticles after the ninth plasma treatment, and the decline in catalytic performance may have been caused by the collapse of the NWs into nanoparticles. The SAED inset in Fig. 7(d) shows that the Co–B NWs were still amorphous after many recycling test experiments. It was thus clear that plasma treatment played a positive role in the regeneration of Co–B NW catalysts.

4. Conclusions

In summary, 1D amorphous alloy Co–B NWs were prepared by using layered liquid crystals as templates. Co–B NWs had a diameter of 35–45 nm and a length of 2–5 μm. To improve CMA catalytic hydrogenation activity, the prepared amorphous alloy Co–B NWs were treated with low-temperature plasma. The results showed that the plasma treatment with appropriate power and time had little influence on the morphology and amorphous structure of Co–B NWs, but it could increase the relative content of Co^0 on the surface, promote the specific surface area, and optimize the types of surface active sites present. These changes were beneficial to the improvement of catalytic hydrogenation performance. In addition, during the catalytic hydrogenation cycling test, the amorphous alloy catalyst inevitably comes in contact with oxygen, leading to partial oxidation of the catalyst surface, which reduces the catalytic hydrogenation performance. Repeated plasma treatment could induce the activity and extend the lifetime of Co–B NWs. This work provides a convenient method for the improvement and regeneration of amorphous alloy catalysts.

Conflicts of interest

The authors declare that there are no conflicts of interest.

Acknowledgements

This study was supported by the Hunan Provincial Natural Science Foundation of China (Grant No. 2021JJ30170, 2021JJ30171) and the Scientific Research Fund of the Hunan Provincial Education Department (Grant No. 21A0580, 21A0584).

References

1 F. Jiang, J. Cai, B. Liu, Y. Xu and X. Liu, Particle size effect in the selective hydrogenation of cinnamaldehyde over supported palladium catalysts, *RSC Adv.*, 2016, **6**, 5541–5551.
2 X. Wang, H. Liang, P. Geng and Q. Li, Recent advances in selective hydrogenation of cinnamaldehyde over supported metal-based catalysts, *ACS Catal.*, 2020, **10**, 2395–2412.
3 J. Wang, M. Jin, Y. Sun and H. Zhang, Pt modified MoO_3 catalyst for electrochemically selective C=O hydrogenation of cinnamaldehyde, *Chem. Commun.*, 2022, **58**, 6721–6724.
4 L. Wang, R. Han, Y. Ma, M. S. Duyar, W. Liu and J. Liu, Spatial location and microenvironment engineering of Pt-CeO_2 nanoreactors for selective hydrogenation of cinnamaldehyde to cinnamyl alcohol, *J. Phys. Chem. C*, 2021, **125**, 22603–22610.
5 X. Chen, H. Cao, X. Chen, Y. Du, J. Qi, J. Luo, M. Armbruster and C. Liang, Synthesis of intermetallic Pt-based catalysts by lithium naphthalenide-driven reduction for selective hydrogenation of cinnamaldehyde, *ACS Appl. Mater. Interfaces*, 2020, **12**, 18551–18561.
6 L. Alfilfil, J. Ran, C. Chen, X. Dong, J. Wang and Y. Han, Highly dispersed Pd nanoparticles confined in ZSM-5 zeolite crystals for selective hydrogenation of cinnamaldehyde, *Microporous Mesoporous Mater.*, 2022, **330**, 111566.
7 X. Wang, Y. He, Y. Liu, J. Park and X. Liang, Atomic layer deposited Pt-Co bimetallic catalysts for selective hydrogenation of α, β-unsaturated aldehydes to unsaturated alcohols, *J. Catal.*, 2018, **366**, 61–69.
8 Z. Iqbal, M. Sadiq, S. Sadiq and K. Saeed, Selective hydrogenation of cinnamaldehyde to cinnamyl alcohol over palladium/zirconia in microwave protocol, *Catal. Today*, 2022, **397–399**, 389–396.
9 K. Wang, X. He, J. Wang and X. Liang, Highly stable Pt–Co bimetallic catalysts prepared by atomic layer deposition for selective hydrogenation of cinnamaldehyde, *Nanotechnology*, 2022, **33**, 215602.
10 J. Zhao, H. Yuan, Y. Gui, X. Li, X. Qin, C. Wei, Y. Liu, G. Wang, L. Zhou and S. Fang, Engineering the interface of Au nanocatalysts with FeO_x for enhanced selective hydrogenation of cinnamaldehyde, *J. Mater. Sci.*, 2021, **56**, 5760–5771.
11 X. Ren, M. Guo, H. Li, C. Li, L. Yu, J. Liu and Q. Yang, Microenvironment engineering of ruthenium nanoparticles incorporated into silica nanoreactors for enhanced hydrogenations, *Angew. Chem., Int. Ed.*, 2019, **58**, 14483–14488.
12 J. Li, Q. Guan, H. Wu, W. Liu, Y. Lin, Z. Sun, X. Ye, X. Zheng, H. Pan, J. Zhu, S. Chen, W. Zhang, S. Wei and J. Lu, Highly active and stable metal single-atom catalysts achieved by strong electronic metal-support interactions, *J. Am. Chem. Soc.*, 2019, **141**, 14515–14519.
13 J. Su, W. Shi, X. Liu, L. Zhang, S. Cheng, Y. Zhang, G. A. Botton and B. Zhang, Probing the performance of structurally controlled platinum-cobalt bimetallic catalysts

for selective hydrogenation of cinnamaldehyde, *J. Catal.*, 2020, **388**, 164–170.

14 H. Xin, W. Zhang, X. Xiao, L. Chen, P. Wu and X. Li, Selective hydrogenation of cinnamaldehyde with $Ni_xFe_{1-x}Al_2O_{4+\delta}$ composite oxides supported Pt catalysts: C=O versus C=C selectivity switch by varying the Ni/Fe molar ratios, *J. Catal.*, 2021, **393**, 126–139.

15 M. Luneau, J. S. Lim, D. A. Patel, E. C. H. Sykes, C. M. Friend and P. Sautet, Guidelines to achieving high selectivity for the hydrogenation of α,β-unsaturated aldehydes with bimetallic and dilute alloy catalysts: a review, *Chem. Rev.*, 2020, **120**, 12834–12872.

16 H. Li, J. He, A. Riisager, S. Saravanamurugan, B. Song and S. Yang, Acid-base bifunctional zirconium N-alkyltriphosphate nanohybrid for hydrogen transfer of biomass-derived carboxides, *ACS Catal.*, 2016, **6**, 7722–7727.

17 H. Li, W. Zhao and Z. Fang, Hydrophobic Pd nanocatalysts for one-pot and high-yield production of liquid furanic biofuels at low temperatures, *Appl. Catal., B*, 2017, **215**, 18–27.

18 H. Li, Y. Li, Z. Fang and R. L. Smith Jr, Efficient catalytic transfer hydrogenation of biomass-based furfural to furfuryl alcohol with recyclable Hf-phenylphosphonate nanohybrids, *Catal. Today*, 2019, **319**, 84–92.

19 Y. Lv, M. Han, W. Gong, D. Wang, C. Chen, G. Wang, H. Zhang and H. Zhao, Fe-Co alloyed nanoparticles catalyzing efficient hydrogenation of cinnamaldehyde to cinnamyl alcohol in water, *Angew. Chem., Int. Ed.*, 2020, **59**, 23521–23526.

20 H. Chen, T. Peng, B. Liang, D. Zhang, G. Lian, C. Yang, Y. Zhang and W. Zhao, Efficient electrocatalytic hydrogenation of cinnamaldehyde to value-added chemicals, *Green Chem.*, 2022, **24**, 3655–3661.

21 H. Li, X. Chen, M. Wang and Y. Xu, Selective hydrogenation of cinnamaldehyde to cinnamyl alcohol over an ultrafine Co-B amorphous alloy catalyst, *Appl. Catal., A*, 2002, **225**, 117–130.

22 J. Zhao, V. Malgras, J. Na, R. Liang, Y. Cai, Y. Kang, A. A. Alshehri, K. A. Alzahrani, Y. G. Alghamdi, T. Asahi, D. Zhang, B. Jiang, H. Li and Y. Yamauchi, Magnetically induced synthesis of mesoporous amorphous CoB nanochains for efficient selective hydrogenation of cinnamaldehyde to cinnamyl alcohol, *Chem. Eng. J.*, 2020, **398**, 125564.

23 H. Li, D. Zhang, G. Li, Y. Xu, Y. Lu and H. Li, Mesoporous Ni–B amorphous alloy microspheres with tunable chamber structure and enhanced hydrogenation activity, *Chem. Commun.*, 2010, **46**, 791–793.

24 W. Wang, P. Liu, K. Wu, K. Zhang, L. Li, Z. Qiao and Y. Yang, Synthesis of Ni–P–B amorphous nanoparticles with uniform size as a potential hydrodeoxygenation catalyst, *New J. Chem.*, 2015, **39**, 813–816.

25 M. Mo, M. Zheng, J. Tang, Q. Lu and Y. Xun, Highly active Co–B, Co–Mo(W)–B amorphous nanotube catalysts for the selective hydrogenation of cinnamaldehyde, *J. Mater. Sci.*, 2013, **49**, 877–885.

26 M. Mo, M. Zhou, M. Xie, L. Han, X. Guo and W. Ding, Tri-component noncrystalline Ni–Cu–B nanotubes with enhanced stability and catalytic performance for hydrogenation of *p*-chlorinitrobenzene, *Catal. Commun.*, 2015, **64**, 66–69.

27 M. Mo, M. Xie, X. Guo, W. Ding and X. Guo, The promoted catalytic hydrogenation performance of bimetallic Ni–Co–B noncrystalline alloy nanotubes, *RSC Adv.*, 2019, **9**, 26456–26463.

28 W. Wei, Y. Zhao, S. C. Peng, H. Y. Zhang, Y. P. Bian, H. X. Li and H. Li, Hollow Ni-Co-B amorphous alloy nanospheres: Facile fabrication via vesicle-assisted chemical reduction and their enhanced catalytic performances, *J. Mater. Chem. A*, 2014, **2**, 19253–19259.

29 B. Jiang, H. Song, Y. Kang, S. Wang, Q. Wang, X. Zhou, K. Kan, Y. Gu, J. Ye, H. Li, Y. Sakka, J. Henzie and Y. Yusuke, A mesoporous non-precious metal boride system: synthesis of mesoporous cobalt boride by strictly controlled chemical reduction, *Chem. Sci.*, 2022, **11**, 791–796.

30 Y. Kang, J. Henzie, H. Gu, J. Na, A. Fatehmulla, B. S. A. Shamsan, A. M. Aldhafiri, W. A. Farooq, Y. Bando, T. Asahi, B. Jiang, H. Li and Y. Yamauchi, Mesoporous metal–metalloid amorphous alloys: the first synthesis of open 3D mesoporous Ni-B amorphous alloy spheres via a dual chemical reduction method, *Small*, 2020, 1906707.

31 Z. Li, S. Tian, H. Wang and H. Tian, Plasma treatment of Ni catalyst via a corona discharge, *J. Mol. Catal. A: Chem.*, 2004, **211**, 149–153.

32 L. Zhang, C. Yang, L. Zhang, H. He, M. Luo, Y. Jia and Y. Li, Application of plasma treatment in preparation of soybean oil factory sludge catalyst and its application in selective catalytic oxidation (SCO) denitration, *Materials*, 2018, **11**, 1609.

33 K. Lin, Y. Lu, S. Du, X. Li and H. Dong, The effect of active screen plasma treatment conditions on the growth and performance of Pt nanowire catalyst layer in DMFCs, *Int. J. Hydrogen Energy*, 2016, **41**, 7622–7630.

34 Y. Zhang, L. Tao, C. Xie, D. Wang, Y. Zou, R. Chen, Y. Wang, C. Jia and S. Wang, Defect engineering on electrode materials for rechargeable batteries, *Adv. Mater.*, 2020, **32**, 1905923.

35 K. Gu, D. Wang, C. Xie, T. Wang, G. Huang, Y. Liu, Y. Zou, L. Tao and S. Wang, Defect-rich high-entropy oxide nanosheets for efficient 5-hydroxymethylfurfural electrooxidation, *Angew. Chem., Int. Ed.*, 2021, **60**, 20253–20258.

36 J. H. Shen and Y. W. Chen, Catalytic properties of bimetallic NiCoB nanoalloy catalysts for hydrogenation of *p*-chloronitrobenzene, *J. Mol. Catal. A: Chem.*, 2007, **273**, 265–276.

37 F. Li, R. Ma, B. Cao, J. Liang, Q. Ren and H. Song, Effect of Co-B supporting methods on the hydrogenation of *m*-chloronitrobenzene over Co-B/CNTs amorphous alloy catalysts, *Appl. Catal., A*, 2016, **514**, 248–252.

38 L. F. Chen and Y. W. Chen, Effect of additive (W, Mo, and Ru) on Ni−B amorphous alloy catalyst in hydrogenation of *p*-

Chloronitrobenzene, *Ind. Eng. Chem. Res.*, 2006, **45**, 8866–8873.

39 Y. Kang, B. Jiang, J. Yang, Z. Wan, J. Na, Q. Li, H. Li, J. Henzie, Y. Sakka, Y. Yamauchi and T. Asahi, Amorphous alloy architectures in pore walls: mesoporous amorphous NiCoB alloy spheres with controlled compositions via a chemical reduction, *ACS Nano*, 2021, **14**, 17224–17232.

40 N. Patel, R. Fernandes and A. Miotello, Promoting effect of transition metal-doped Co–B alloy catalysts for hydrogen production by hydrolysis of alkaline $NaBH_4$ solution, *J. Catal.*, 2010, **271**, 315–324.

41 X. Chen, H. Li, H. Luo and M. Qiao, Liquid phase hydrogenation of furfuryl alcohol over Mo-doped Co-B amorphous alloy catalysts, *Appl. Catal., A*, 2002, **233**, 13–20.